Evaporation Induced Capillary Siphoning Through Hydraulically Connected Porous Domains: the Vedernikov-Bouwer Model Revisited

Anvar Kacimov, ORCID ID: orcid.org/0000-0003-2543-3219

Yurii Obnosov, ORCID ID: orcid.org/0000-0001-9220-7989

Dani Or

Submitted to Transport in Porous Media (Springer) on October 8, 2018 as manuscript TiPM-D-18-00549

first set of referees comments received on January 14, 2019;

revised version submitted: on March 23, 2019;

Address for correspondence:

Prof. Kacimov A.R.,
Department of Soils, Water and Agricultural Engineering
Sultan Qaboos University Al-Khod 123, PO Box 34 Sultanate of Oman
Tel (968) 24141-1227 Fax (968) 24413-418
Emails: anvar@squ.edu.om
akacimov@gmail.com
Omani page:
https://www.squ.edu.om/agr/Departments/Soils-Water-and-Agricultural-Engineering/Faculties/Prof-Anvar-Kacimov

Evaporation Induced Capillary Siphoning Through Hydraulically Connected Porous Domains: the Vedernikov-Bouwer Model Revisited

A.R. Kacimov[1],Yu.V.Obnosov[2], D. Or[3]

[1]Sultan Qaboos University, Department of Soils, Water and Agricultural Engineering, Muscat, Oman,

anvar@squ.edu.om

[2]Institute of Mathematics and Mechanics, Kazan Federal University, Kazan, Russia

yobnosov@gmail.com

[3]Department of Environmental Systems Science, ETH Zurich, Switzerland

dani.or@env.ethz.ch

Abstract

Evaporation-driven wicking of soil water through porous domains with contrasting hydraulic properties, is studied analytically by conformal mappings and compared to numerical solutions. Initially, the connected rectangular domains are fully saturated. The first rectangle, G_p, is comprised of a coarse-textured porous medium with large permeability and low capillary forces. Evaporation induced capillary flow pulls water horizontally across the domains to the surface of fine-textured rectangular domain, G_z, through an interfacial hydraulic exchange region that shrinks with time. The flow field in G_z is 2-D and is analytically expressed by the Vedernikov-Bouwer model, that assumes a constant hydraulic conductivity for pressure heads higher than the air-entry value. The rate of 1-D drop of the phreatic surface in G_p is proportional to the evaporation rate (decreasing with time) from the G_z surface. The complex potential domain G_w, "shrinks" with time, and at any time instance, it is conformally mapped onto G_z via two auxiliary planes using the Schwarz-Christoffel and Mobius transformations. The resulting Cauchy problem for an integro-differential equation with respect to an affix of the conformal mapping is solved using numerical algebra routines. A similar capillary coupled flow problem was numerically simulated using

HYDRUS2D considering 2-D flow in both G_p and G_z. New insights into process dynamics is gained from a solution of an auxiliary optimization for a vertical imbibition in a column brought in contact with a water table where particle size (linking capillarity and permeability) is used as a control variable and counter-gravity front propagation dynamics as criteria.

Key words: counter gravity imbibition; stages of evaporation; 2-D potential flow; complex potential; HYDRUS simulations.

1. Introduction

A common pattern of alluvial soil deposits in coastal catchments of the Gulf (Oman and UAE, see e.g. Schulz et al., 2015), is characterized by recurrence of sands (often sand dunes) separated by flat silty sabkhas (as illustrated in Fig.1a and indicated by $Zone_f$ and two adjacent $Zones_c$) This pattern is also illustrated in images of sabkha and sand landscapes from Nambia, Central Asia, Oman and UAE (see for instance McKay et al., 2016). The topsoil in $Zones_f$ is often wet throughout the year with intensive evaporation due to the relatively shallow water table (Kacimov and Obnosov, 2006, Singer et al., 2001). In the adjacent sandy $Zones_c$, a few tens to hundreds meters away from $Zones_f$ (see the image 1 in the Supplementary Electronic File, SEF) with a similar water table depth, the topsoil is dry and wets only by infrequent rain events and dries out in a few days. This disparity in surface conditions across short distances carries several hydrological, ecological and civil engineering implications. These include aspects of sea water intrusion, water balances at local and catchment scale, a resulting mosaic of vegetation (for example, halophites in $Zones_f$ versus irrigated crops-ornamental plants in $Zones_c$), and cracking/damping of infrastructure foundations in $Zones_f$, among others (Kacimov et al., 2009). Direct measurements (see image 1 in SEF) record an abrupt increase in soil moisture content when trespassing the boundary between even a flat $Zone_c$ to $Zone_f$. At a smaller (sub-meter) scales, a

similar mosaic of fine silty blocks and coarse sand have observed and investigated by Al-Ismaily (2013).

There is growing interest in the roles of geomorphology, sedimentology, hydrology, and salt transport in the functioning of sensitive coastal systems of sabkha-sand landforms in Oman-UAE due to the following:

- Land available for crop fields is limited, coastal catchments are populated by farmers;
- Infrastructure in support of tourist industry (buildings, roads, pavement, etc.) and rapid urban encroachment in coastal zones (Muscat, Sohar, Abu-Dhabi and other cities of the region);
- During field trips, soil science-hydrology students at SQU are exposed to flummoxing moisture content patterns in coastal catchments of Oman, i.e. understanding flow regimes in Fig.1a,b has a pedagogical value;
- The desert ecology, especially, the ecotones (see image 3 in SEF illustrating shrubs grow on minidunes) in plant cover of $Zones_c$ - $Zones_f$ is determined by water and solute fluxes through the topsoil;
- See water intrusion and water logging of coastal zones requires quantification of hydrological balances, especially, the evaporative losses of groundwater resources from the wet surfaces.

(El-Sheikh et al., 2010, Schulz et al., 2015, Yechieli and Wood, 2002).

Fine-textured regions (often topographic depressions or planes) interacting with sands, similar to landforms depicted in Fig.1c and image 1 in SEF are common in Central Asia (called “takyrs”, “solonchaks”, “shors” and “solonets”, Erley, 2012, Platonov, 1934, Yechieli and Wood, 2002). These landforms exhibit unique and rich patterns of soil water/groundwater fluxes in laterally adjacent coarse-fine soil massifs (Babaev, 1994, Gael and Smirnova, 1999, Kunin, 1959, Ogar,

2001, Orlovsky et al. 2012, Zonn and Esenov, 2012)." The Dokuchaev school in soil sciences (Rode, 1947), Soviet hydrologists and irrigation-water supply engineers (e.g. Babaev, 1994, 2012, Kunin, 1959, Platonov, 1934) studied soils and hydrology of takyrs and adjacent sands both analytically and holistically.

To represent the unique lateral hydrological interactions emerging in such interspaced landforms, that occur in arid regions with high evaporative demand, we propose a simple conceptual model (shown as a vertical cross-section of Fig.1b). We consider two rectangular porous domains that are hydrologically-coupled in a manner that represents the interfaces that may occur at different scales in the sabkha-sand dunes landscapes (see Fig. 1a). Unlike the standard vertically stratified soil horizons often at the scale of pedons (Pachepsky and Hill, 2017) and associated 1-D vertical vadose zone fluxes in deserts (Chen et al., 2018, Wang et al., 2017, Zhang et al., 2018), the properties of the composite domains in Fig.1b are assumed to be uniform with depth but the texture vary among the domains in the lateral direction (perpendicular to $\vec{g}$). The moisture fluxes are indicated by arrows in Fig.1a,b. Physically similar multidimensional fluxes in texturally-contrasting porous media have been engineered as "smart root zones" at scales of tens of centimeters (Al-Maktoumi et al., 2014), and demonstrated that overall evaporation rates from the composite domains were significantly lower than equivalent homogeneous soils with potentially important agro-engineering perspectives for growing plants in arid environments. We note certain similarity in the designs of "smart root zones" of Al-Maktoumi et al. (2014) in agronomic applications and Beyhaghi et al. (2014) in chemical engineering; in both cases ascending water fluxes in porous media are optimized with capillarity as a driving mechanism We use the terminology from Blunt (2017, see e.g. pp.78, 104, 115, 126, 189, 353) for a spontaneous imbibition (always opposed by the matrix Darcian resistance) as a process in which a wetting phase (water) displaces a non-wetting air; our models are macroscopic (no analysis on a pore scale).

The phenomenon of 1-D evaporation from a horizontal layered soil has been thoroughly investigated (Shokri et al. 2010, Assouline et al., 2014, Gardner and Fireman, 1958, Willis, 1960). In contrast, the vertical interface *BA* and horizontal infiltration-exfiltration segments B_1B-*BC* in Fig.1b render the flow essentially 2-D and transient a drastically different scenario that the 1-D evaporation regime. Several studies have been conducted to investigate two and three dimensional capillary wicking (see Patnaik, et al. 2006; we use this term interchangeably with "siphoning") and associated solute transport from such interacting porous media consisting of coarse and fine domains (Bechtold et al., 2011, Bergstad et al., 2018, Lehmann and Or, 2009, Lehmann et al., 2008, Or, 2008, Shokri and Or, 2011, 2013, Shokri et al., 2010) very similar to conceptual domains sketched in Fig.1a,b. A pragmatic question arising from these studies is the potential of quantifying such wicking using simple mathematical models (analytical and numerical) that could represent the transient flow and flux conditions expected in natural systems and the 2-D flow behavior across hydraulically interacting domains with a contrast in hydraulic and capillary properties.

Transient capillary lateral flows with evaporation from texturally heterogeneous soils has been studied in applications to the hydrology of regions in the Gulf, geotechnical engineering, and vegetation response (Al-Ismaily, 2013, Kacimov et al., 2010, Kacimov and Obnosov, 2013). The corresponding path-, stream-, streak -lines and Darcian velocities are controlled by capillarity, gravity, transpiration and viscous resistance (saturated-unsaturated hydraulic conductivity) of the porous skeleton and boundary conditions, which describe the interaction of the skeleton with the atmosphere (evaporation) and free water body (e.g. dam reservoir). Scrutiny of soil water motion in composites like one in Fig.1b is also helpful for assessment of nutrients' transport to the plant roots, migration of agrochemicals on the catchment scale, temperature fields of the top soil, mechanical stability of soil-covered slopes to seepage-induced internal erosion (suffusion), among others.

Motivated by the arid-zone examples listed above, we seek to solve two types of transient problems, 2-D and 1-D macroscopic single phase flows. In the analytical solutions, we employ a special type of constitutive relations for the soil-water retention curve and water permeability functions, viz. two step-functions. In the numerical solutions by the HYDRUS2D we use the Van Genuchten parametric model. Both, analytical and numerical models bear all the limitations discussed in Blunt (2017, p.353).

The formalism of holomorphic functions (Polubarinova-Kochina, 1977, hereafter abbreviated as PK-77, Strack, 2017) is used in section 2 to study the evaporative 2-D flow in G_z. We assume that this rectangle is always fully saturated. The total hydraulic head and pressure head in G_z obey the Laplace equation. In Section 3, the Richards equation is solved by FEM (Simunek et al., 2016) for a saturated-unsaturated flow in both rectangles of Fig.1b. In Section 4, we use the Vedernikov-Bouwer (VB) model in 1-D ascending flow (wicking) through a homogeneous column, the texture of which is analytically optimized with an objective of a fastest or most extensive imbibition from a horizontal zero-pressure isobar and soil particle size as a control variable.

2. Analytical Solution for 2-D Evaporation Driven Flows

2.1 *Theoretical considerations*

We begin by framing the problem for the analysis. In Fig.1b, a coarse-textured rectangle A_3B_1BA, G_p has a saturated hydraulic conductivity k_1. Along a segment AB, G_p vertically contacts another rectangle $ABCD$, G_z, made of a fine-textured material of conductivity k_2. We assume that the sides B_1A_3, A_3D and DC are impervious. Kacimov et al. (2017) experimentally measured and modeled 1-D desiccation and temperature field in a composite domain similar to one depicted in Fig.1b. In natural systems, interacting domains shown in image 1 of the SEF and conceptualized in Fig.1b, are subjected not only to episodic and relatively short rainstorms, but in some regions to

more frequent irrigation pulses. After such wetting events, radiative energy intercepted on the top soil (B_1BC) that interacts with hot and dry air induces evaporation. For simplicity, we consider soil water salt free to avoid complications of salt precipitation that could affect evaporation, we focus on bare soil processes with no plants hence no water losses by transpiration.

Consequently, a transient 2-D flow takes place in Fig.1b due to a lateral transfer of soil water between G_p and G_z. Siphoning drives water horizontally from A_3B_1BA to $ABCD$. Darcian resistance of the soils impedes flow in G_z and gravity helps drainage in G_z while resists exfiltration (evaporation) in G_p. It is noteworthy that similar "canonical" rectangular domains with alternating boundary conditions along the sides of the rectangle are considered in 2-D two-phase flow models (Meng et al., 2016).

We assume that in G_p a standard 1-D vertical flow takes place. The segment B_1B becomes dry relatively fast (see e.g. Hellwig, 1973) due to high permeability and low capillarity of the coarse-textured compartment. In applications to dune hydrology, the domain boundary is at the dune edge (as marked by the dashed curve BB_2 in Fig.1b) suggests that evaporation from the dune slope would be even less than from a horizontal segment BB_1. A receding (horizontal) phreatic surface A_2A_1 in G_p has its locus described by the function $a(t)$ (Fig.1b) with hydrostatic pressure head, $p_1(t,y)=a(t)-y$. The rate of drawdown, da/dt, of A_2A_1 decreases with time. We assume that G_z in Fig.1b remains very wet and keeps evaporating a constant-density water through a rigid skeleton (compaction and cracking are ignored). G_z receives water from A_3B_1BA through a vertical segment AA_1, which "shrinks" with time until $a(T)=0$, where T is extinction time. At $t>T$ a genuine (desaturation –desiccation-mechanical deformation) of G_p takes place. At $0<t<T$, flow in G_z is 2-D with a curved phreatic surface A_1M.

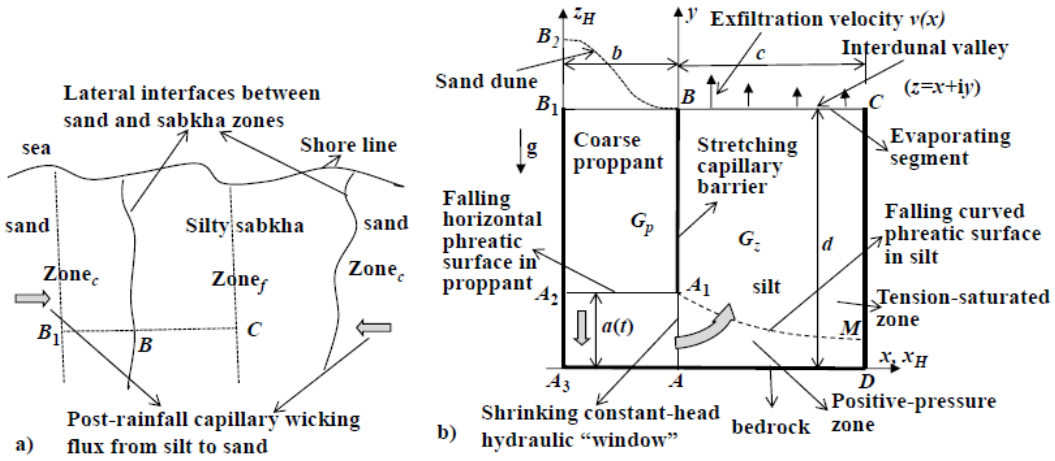

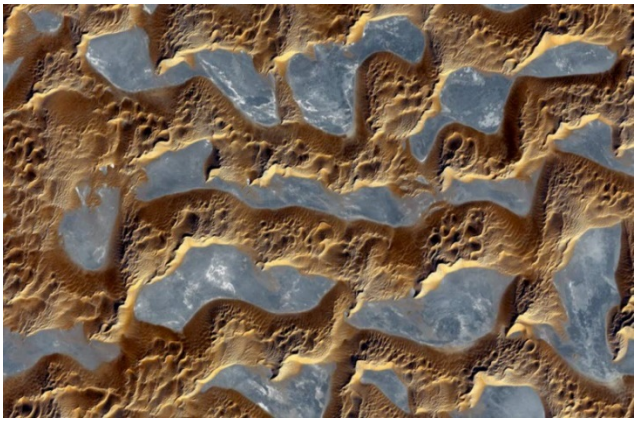

c) d)

Fig.1. Definition sketch, image and photos of spatial zonation in soil texture in arid climates. Plan view, soil surface of a fine-textured Zone$_f$ is wet, coarse-textures soil surface in Zones$_c$ is dry (a); vertical cross-section of two adjacent porous compartments, G_p is a highly porous rectangle in which a horizontal water table drops in 1-D manner and in G_z 2-D tension-saturated transient VB flow takes place (b); interdunal depression in Nambia (c); NASA satellite image visualizing textural intermittence of arid land (d);

We introduce Cartesian coordinates *xAy*, the ordinate axis coincides with the interface between the two rectangles in Fig.1b. The widths of the G_p and G_z are b and c, their height is d. The elevation, $a(t)$, of A_1A_2 above the abscissa axis is a part of solution. For coarse-textured domain of

low capillarity the drop of A_1A_2 causes instantaneous desaturation of the pore space above this falling free surface (in the vernacular of groundwater hydrology, the specific yield in G_p coincides with the soil porosity). We ignore the capillary fringe above A_1A_2. Without any loss of generality, we also ignore gas flow and evaporation (both through liquid films and via a gaseous phase) from A_1A_2 to BB_1 and assume that water evaporates from BC only[1]. Most sabkhas are flat landforms, which are bordered by sandy dunes, hillocks and nebkhas (Babaev, 2012, Beckeley et al., 2008, Orlovsky et al., 2012, Zonn and Esenov, 2012). Therefore if the boundary of a coarse zone (BB_2 in Fig.1a) is not horizontal but rather curved as a dune slope then even less evaporation will take place from it.

The evaporation rate from BC is not only transient but also not uniform along BC. In other words, the exfiltration (evaporation) flux from BC is part of the solution, similar to the Toth (2009) model, in which a 2-D saturated flow element (a rectangle or trapezium) also is bounded from above by an isobar-water table (capillary fringe is ignored) with an *aposteriori* reconstructed infiltration-exfiltration flux (see also Strack, 1978 for flow elements without confining bedrock in the Toth model). Because $k_1/k_2>>1$ there is no viscous resistance to vertical drainage of water in G_p.

In the Vedernikov (1939) model (see also Bouwer, 1964, Kacimov, 2006, PK-77, Samal and Mishra, 2017, Youngs, 2012, Youngs et al., 1993), G_z in Fig.1b has a positive pressure zone beneath A_1M and a "capillary fringe" between A_1M and BC. In the fringe, the pores are fully occupied by water but pressure is negative (water is "tension-saturated"). Vedernikov's model assumed that the hydraulic conductivity equals k_2 in the whole G_z. Bouwer (1964) substantiated Vedernikov's steady-state 2-D analytical solutions by addressing three types of tension-saturated flows: purely vertical descending through a thin low-permeable layer into a highly-permeable

[1] We can easily take into account evaporation in G_p as well. Namely, an ascending evaporative flux from A_1A_2 to BB_1 which is proportional to d-$a(t)$ can be considered (see e.g, Kacimov and Obnosov, 2013). For this generalization the PK-77 exponential or algebraic evaporation functions can be used.

substratum (seepage through a liner or colmatage layer of a soil channel), quasi-horizontal in a capillary fringe of an unconfined aquifer, and quasi-vertical descending (seepage from a soil channel with a phreatic surface having a capillary fringe, which - in a vertical cross-section - is a thin vertical strip adjacent to the phreatic line). Below, we extend the Bouwer catalogue and examine flow which can be classified as U-turning, ascending-descending, tension-saturated. We note that mathematically similar GA-VB-type model for 2-,3-D tension-saturated flow from one isobar to another has been used by Benner and Petsev (2018), Elizalde et al. (2015), Mendez et al. (2009), Xiao et al. (2012).

The segment A_1B (a contact line between a completely desaturated portion of the medium and a tension-saturated fine zone) is also a no-flow boundary (see Kacimov, 2006 for more details). We assume that along *BC* the soil water pressure is constant during the whole process of evaporation. The total evaporation rate, $Q(t)$, from *BC* to the atmosphere decreases with time because of the drawdown of $a(t)$.

2.2 *Conformal Mappings*

We assume that the flow is Darcian and –recall that the- tension-saturated, G_z is homogeneous and isotropic. We introduce a complex physical coordinate $z=x+iy$. The total hydraulic head, $h(t,x,y)$, is related to the Darcian velocity, $\vec{V}(t,x,y)$ as:

$$\vec{V} = -k_2 \nabla h \,. \tag{1}$$

Next, we introduce the complex potential $w(t,x,y) = \phi + i\psi$, where $\phi = -k_2 h$ is the velocity potential, and ψ is the stream function. Both ϕ and ψ are harmonic functions at each fixed *t*. The pressure head is $p(t,x,y) = -\phi / k_2 - y + c_1(t)$, where $c_1(t)$ is expressed from the physical conditions at point *A* in Fig.1b. We select *A* as a fiducial point because the complex potential is defined up to an arbitrary complex constant (see PK-77). At this point, we set $w=0$. We have

already assumed that the porous medium has no capillarity and no Darcian resistance and hence the line A_2A_1 is a horizontally-translating zero-pressure isobar. We also recall that in a real dune (below the curve BB_2 in Fig.1b) the post rain drainage front is often more complicated due to complex microstratification of dune core as described by the classics of dune hydrology in the deserts of North Africa (Bagnold, 1941) and measured in dunes in of Israel (Breckle et al., 2008).

Along the shrinking segment AA_1 $\phi = 0$. This is a common assumption along the reservoir boundaries or interfaces between coarse (rip-rap, gravel, sand) shoulders and cores of earth-filed dams (Kacimov and Obnosov, 2012, PK-77). Clearly, at point A the pressure head $p_A = a(t)$. Consequently, $c_1(t)=a(t)$ and $p = -\phi / k_2 - y + a(t)$ in G_z. Along ADC we set $\psi = 0$. Then along A_1B the stream function $\psi = Q(t)$. Along BC the pressure head $p = -p_{BC}$, $p_{BC} < p_c$ where p_c is a given positive constant. As will be evident from our solution, there are no mathematical constraints to consider an arbitrary function $p_{BC}(t)$ as a boundary condition at the outlet of G_z. Thus, along BC:

$$\phi = k_2 (p_{BC} + a(t) - d) = k_2 f(t) . \qquad (2)$$

In order to maintain flow from AA_1 to BC the inequality $f > 0$ or $p_{BC} + a(t) > d$ should hold.

We note that the soil constant p_c is equivalent to the thickness of the capillary fringe under static conditions (see PK77), i.e. the evaporating side of G_z is not too dry. Bouwer (1964) related p_c to the unsaturated conductivity function (Bouwer's eqn.5), for which he used the parameters of Gardner's algebraic functions. Bouwer and PK-77 reported p_c values of fine-textured soils in the range of tens-hundreds of centimeters. As soon as $\phi_{AA_1} < 0$, feeding of G_z from G_p stops because the whole line of contact AB becomes a capillary barrier ("hydraulic locking"). Then a genuine (2-D) desaturation of G_z starts (see Assouline et al., 2014), for which the VB model becomes unusable.

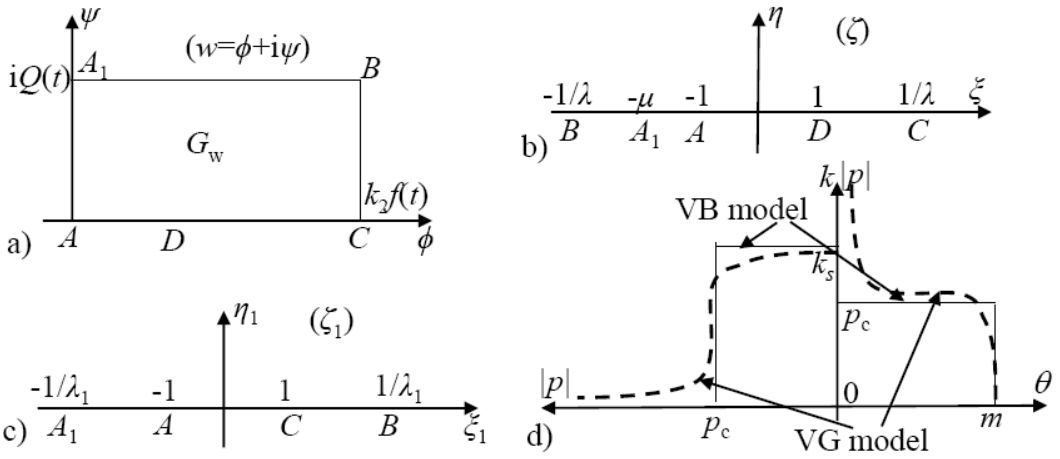

Fig.2 Complex potential domain $G_w(t)$ corresponding to G_z (a), image of G_z in the ζ-reference plain (b); image of G_w in the ζ_1-reference plain (c); Soil-water constitutive relations (water retention curve and unsaturated conductivity as function of matrix potential) in VB and VG models (solid and dashed lines) (d).

The flow domain G_z is a flow tube, imaged by a rectangle G_w in the complex potential plane (Fig.2a). We emphasize that both sizes of G_w are to be found (with time this rectangle shrinks in sizes).

In order to find $Q(t)$, $a(t)$, $f(t)$ and $\psi(x)$ along BC we map conformally G_w onto G_z using two auxiliary planes $\varsigma = \xi + \mathrm{i}\eta$ and $\varsigma_1 = \xi_1 + \mathrm{i}\eta_1$ shown in Fig.2b and Fig.2c, correspondingly. The mapping of G_z onto the upper half-plane $\varsigma > 0$ with the correspondence of the vertexes $B \to -1/\lambda$, $A \to -1$, $D \to 1$, $C \to 1/\lambda$, where $0 < \lambda < 1$, is given by the Schwarz-Christoffel formula:

$$z(\zeta) = \frac{c}{2} + \frac{c}{2K(\lambda)} \int_0^{\zeta} \frac{\mathrm{d}t}{\sqrt{(1-t^2)(1-\lambda^2 t^2)}} = \frac{c}{2} + \frac{c}{2K(\lambda)} F(\arcsin\zeta, \lambda), \qquad (3)$$

where $F(\arcsin\zeta,\lambda)$ and $K(\lambda)$ are incomplete and complete elliptic integrals of the first kind (see Abramowitz and Stegun, 1969, formulae 17.2.7, 17.3.1). From eqn.(3), we have $z(1/\lambda)=c+\mathrm{i}d$ and $F(\arcsin(1/\lambda),\lambda)=K(\lambda)+\mathrm{i}K'(\lambda)$ that gives

$$\frac{K'(\lambda)}{2K(\lambda)}=\frac{d}{c}, \qquad (4)$$

where $K'(\lambda)=K(\lambda')$, $\lambda'=\sqrt{1-\lambda^2}$. The right hand side in eqn.(4) is known and we immediately determine a time-independent constant λ using the standard **FindRoot** routine of Wolfram's (1991) *Mathematica*.

The image of point A_1 in the half-plane of Fig.2b is $\varsigma=-\mu$. The positive time-dependent parameter μ satisfies the condition $1/\lambda>\mu>1$ and is found directly from eqn.(2) and formula (1.2.64.1) from Prudnikov et al. (2002) as:

$$a(t)=\frac{c}{2K(\lambda)}\int_{-\mu(t)}^{-1}\frac{\mathrm{d}\tau}{\sqrt{(\tau^2-1)(1-\lambda^2\tau^2)}}=\frac{c}{2K(\lambda)}F\left(\arcsin\left(\frac{\sqrt{\mu(t)^2-1}}{\lambda'\mu(t)}\right),\lambda'\right). \qquad (5)$$

We recall that the complex coordinate of point A_1 in G_z is $z=\mathrm{i}\,a(t)$ (Fig.1b).

We map G_w onto the upper half plane $\varsigma_1>0$, with the correspondence of the vertexes $A_1\to-1/\lambda_1$, $A\to-1$, $C\to1$, $B\to1/\lambda_1$, where $0<\lambda_1<1$. The corresponding Schwarz-Christoffel formula results is:

$$w(\zeta_1)=\frac{k_2 f}{2}+\frac{k_2 f}{2K(\lambda_1)}\int_0^{\zeta_1}\frac{\mathrm{d}t}{\sqrt{(1-t^2)(1-\lambda_1^2t^2)}}=\frac{k_2 f}{2}+\frac{k_2 f}{2K(\lambda_1)}F(\arcsin\zeta_1,\lambda_1). \qquad (6)$$

As $w(1/\lambda_1)=k_2 f+\mathrm{i}Q$ (see Fig.2a), then from eqn.(6) and the equality $F(\arcsin(1/\lambda_1),\lambda_1)=K(\lambda_1)+\mathrm{i}K'(\lambda_1)$ follows:

$$\frac{K'}{2K}=\frac{Q}{k_2 f}, \qquad (7)$$

where $K = K(\lambda_1)$, $K' = K(\lambda_1')$, and $\lambda_1' = \sqrt{1-\lambda_1^2}$. Unlike eqn.(4), the right hand side of eqn. (7) is still unknown and λ_1 depends on time.

Next, the ς-half-plane (Fig.2b) is mapped onto ς_1-half-plane (Fig.2c). This is done by the Mobius transformation which is uniquely defined by fixing the relation of three pairs of points: $-1/\lambda \to 1/\lambda_1$, $-1 \to -1$, $1/\lambda \to 1$. Then the mapping function is determined from the following relation :

$$\frac{\varsigma + 1/\lambda}{\varsigma + 1}\frac{1/\lambda + 1}{2/\lambda} = \frac{\varsigma_1 - 1/\lambda_1}{\varsigma_1 + 1}\frac{2}{1 - 1/\lambda_1}. \tag{8}$$

Due to the correspondence of points A_1 in the two reference half-planes, we put $\varsigma = -\mu$ into the left hand side of eqn.(8) and $\varsigma_1 = -1/\lambda_1$ into the right hand side of this equation and obtain

$$\frac{1-\mu}{\mu - 1}\frac{\lambda}{2\lambda}\frac{1+\lambda}{2\lambda} = \frac{4\lambda_1}{(1-\lambda_1)^2}. \tag{9}$$

Eqn.(9) is a quadratic equation with respect to λ_1. The root of this equation, satisfying the condition $0 < \lambda_1 < 1$, is given by the formula:

$$\lambda_1 = \frac{2 + s - 2\sqrt{s+1}}{s}, \quad s = \frac{1-\mu}{\mu - 1}\frac{\lambda}{2\lambda}\frac{1+\lambda}{2\lambda}. \tag{10}$$

The rate of water drainage from G_p (see Fig.1b) is

$$Q(t) = -m_1 b \frac{\mathrm{d}a(t)}{\mathrm{d}t}, \tag{11}$$

where m_1 is drainable porosity of the porous medium. The same quantity $Q(t)$ should be exfiltrated as evaporation from BC in G_z (where – we remind – there is no change of soil water storage due to tension-saturation).

A mass-balance principle now combines eqns.(11), (7) and (2):

$$-\frac{2bm_1}{k_2}\frac{K(\lambda_1)}{K'(\lambda_1)}\frac{\mathrm{d}a(t)}{\mathrm{d}t} - a(t) = p_{BC} - d, \quad a(0) = a_0, \tag{12}$$

The initial condition of the Cauchy problem to eqn.(12) is $a_0=d$. This condition reflects full saturation of the whole rectangle G_p at t=0 and broaching of BC at this instance. Darcian flows have no inertia and therefore a_0 in eqn. (12) can be selected arbitrary in the interval $0<a_0<d$ at any time moment $t > 0$. The "falling head" eqn.(12) apparently resembles ones used in permeametry of soil columns or Green-Ampt (abbreviated as GA) 1-D infiltration from a ponded soil surface where Darcian seepage is 1-D (see PK-77). Eqn.(12) is a nonlinear 1-st order ODE with respect to $a(t)$ and $\lambda_1(t)$ is determined by eqn.(10) and μ is related to $a(t)$ through the elliptic integral in eqn. (5).

For practical computations, we used the Leibnitz rule of differentiation in eqn. (5) and transformed eqn.(12) into an equation with respect to the affix $\mu(t)$ of our conformal mapping, rather than $a(t)$:

$$\frac{2bm_1}{k_2}\frac{c\,K(\lambda_1[\mu(t)])}{K'(\lambda_1[\mu(t)])K(\lambda)}\frac{\mathrm{d}\,\mu(t)}{\mathrm{d}\,t}\frac{1}{\sqrt{(\mu^2(t)-1)(1-\lambda^2\mu^2(t))}}+\frac{c}{2K(\lambda)}\int_1^{\mu(t)}\frac{\mathrm{d}\,\tau}{\sqrt{(\tau^2-1)(1-\lambda^2\tau^2)}}=d-p_{BC}, \qquad (13)$$

where eqn.(10) is still involved via the arguments of the complete elliptic integrals $K(\lambda_1)$ and $K'(\lambda_1)$. The initial condition for eqn.(13) is $\mu(0)=\mu_0$, where μ_0 is found for a given a_0.

We used *Mathematica* to solve the integro-differential equation (13). We introduced dimensionless quantities: $(a^*, b^*, d^*, p_{BC}{}^*, t^*, V^*, Q^*)=(a/c, b/c, d/c, p_{BC}/c, tk_2/(m_1c), V/k_2, Q/(k_2c))$. For the sake of brevity we dropped the asterisks for dimensionless quantities. Numerically, we proceeded as following. First, for a given d we found λ from eqn.(4) using the **FindRoot** routine of *Mathematica.* Next, we specified a_0 (below as $0.99d$) and found μ_0 from eqn.(5) by the **FindRoot** routine of *Mathematica.* Next, we used the **EllipticK** and **EllipticF** routines of *Mathematica* to evaluate the complete and incomplete elliptic integrals whose arguments involved the function $\mu(t)$ to be found. Next, we solved eqn. (13) by the **NDSolve** routine (the Runge-Kutta integration) of *Mathematica*. Next, we used again eqn.(5) and by the **FindRoot** evaluated the root of the equation $a(t)=0$, i.e. the extinction time T when all pore water (originally stored in G_p) is

devoured by G_z. Finally, in Fig.3 we plotted $a(t)$ for d=0.75, p_{BC}=1, and b=0.125, 0.25, 0.5 (curves 1-3, correspondingly). From Fig.3, we see that the thinner the sand compartment, the faster it dries out. Also, the rate of drainage and, hence, the rate of evaporation (slope of curves 1-3) decreases with time.

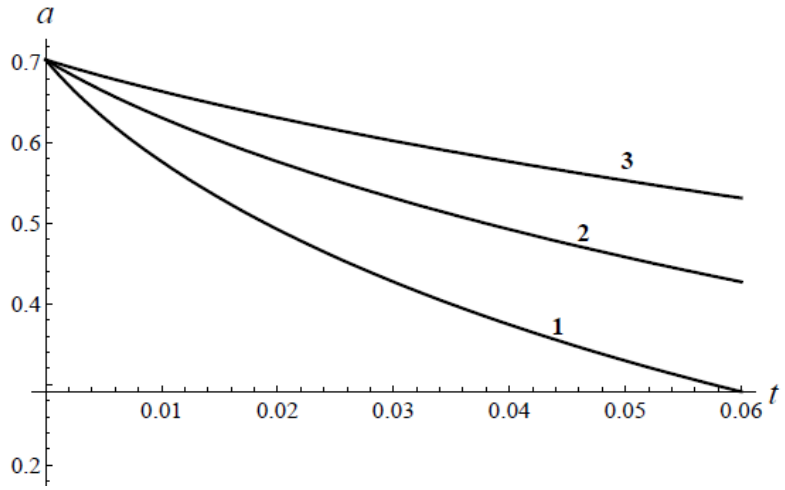

Fig.3. Dimensionless saturated depth a in G_p as a function of dimensionless time, t, for d =0.75, p_{BC}=1 and three widths of the coarse rectangle b=0.125, 0.25, and 0.5 (curves 1-3 correspondingly).

We recall (see PK-77) that dw/dz=u-iv where $u(x,y,t)$ and $v(x,y,t)$ are the horizontal and vertical component of the vector $\vec{V}(t,x,y)$ in eqn.(1). Therefore, by differentiation of eqns.(3) and (6) we obtain $V(\varsigma_1)=u-\mathrm{i}v=\mathrm{d}w/\mathrm{d}z=\mathrm{d}w/\mathrm{d}\varsigma_1/\left(\mathrm{d}\varsigma/\mathrm{d}\varsigma_1\cdot\mathrm{d}z/\mathrm{d}\varsigma\right)$

$$V(\varsigma_1)=\frac{\lambda k_2 fK(\lambda)}{4cK(\lambda_1)}\sqrt{\frac{(1-\varsigma^2)(1-\lambda^2\varsigma^2)}{(1-\varsigma_1^2)(1-\lambda_1^2\varsigma_1^2)}}\frac{\left[\left((1+\lambda)(1-\lambda_1)+4\lambda_1\right)\varsigma_1+(1+\lambda)(1-\lambda_1)-4\right]^2}{(1-\lambda^2)(1-\lambda_1^2)}, \qquad (14)$$

which is complex conjugated with a complexified Darcian velocity V_D=u+i v.

We note that from eqn. (8) the relation between two reference variables is:

$$\varsigma(\varsigma_1)=\frac{\left((1+\lambda)(1-\lambda_1)+4\lambda\lambda_1\right)\varsigma_1+(1+\lambda)(1-\lambda_1)-4\lambda}{\lambda\left[\left((1+\lambda)(1-\lambda_1)+4\lambda_1\right)\varsigma_1+(1+\lambda)(1-\lambda_1)-4\right]} \qquad (15)$$

We plot the distribution of velocity along *BC* for a fixed G_z (i.e. a fixed λ) at a certain time t_c in the following manner. From eqn.(3) we find $x(\xi) = \mathrm{Re}[z(\xi)]$. Next, from eqn.(13) we find $\mu(t_c)$. Then from eqn.(5) we evaluate $a(t_c)$. Next, from eqns. (9)-(10) we calculate λ_1. Eventually, we use the *Mathematica* routine **ParametricPlot** to plot a parametric curve $\{x[\xi(\xi_1)], v[\xi_1, \xi(\xi_1)], 1 < \xi_1 < 1/\lambda_1\}$ and $v[\xi_1, \xi(\xi_1)]$ are found from eqns.(15) and (14), correspondingly.

3. HYDRUS2D Numerical Simulations

In this Section, we simulate flow conditions similar to those in Fig.1b by the HYDRUS2D (Šimůnek et al., 2016), a FEM code which numerically solves the Richards equation for saturated-unsaturated soils. We have used several default HYDRUS options: time step controls, the VGM capillary pressure and phase permeability functions (sketched as dashed lines in Fig.2d for comparison with corresponding functions in the VB model of Section 2 shown as solid lines; k_s is saturated conductivity), and the Soil Catalogue. We note that Youngs (2012) and Youngs et al. (1993) discussed in details the relation between the VB model having step-functions (Fig.2d) and the Gardner model which assumes a particular class of continuous soil constitutive functions.

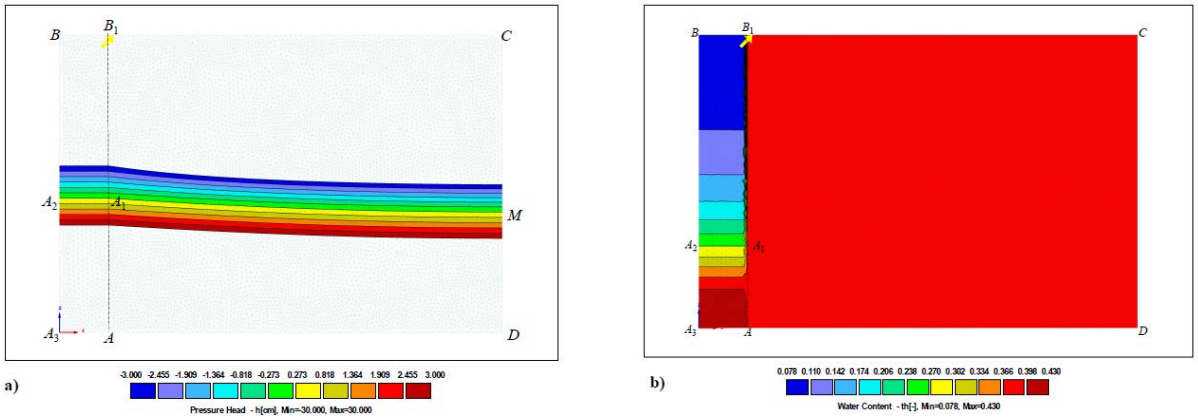

Fig.4. Pressure head contours at early stage (*t*=1 day) of drainage of a coarse and imbibition into the fine-textured rectangular domain a); moisture content contours at late stage (*t*=20 day) b).

The HYDRUS Cartesian coordinates are $x_H A_3 z_H$ in Fig.4 a,b, (the origin of coordinates in Fig.4 is shifted distance b to the left as compared with Fig.1b; a vertical dashed line indicates the interface between two porous rectangles). First, we simulated for 45 days. An initial (at t=0) pressure head in both G_z and G_p was hydrostatic. We selected b=5 cm, c=40 cm, d=30 cm, HYDRUS sand as the porous medium, for which the Soil Catalogue of HYDRUS gives k_1=712.8 cm/day, m_1=0.43, α = 0.145 1/cm, n =2.68, and clay (not silt) as the fine medium of G_z, for which k_2=4.8 cm/day, m_2=0.38, α= 0.008 1/cm, n=1.09. We note that clay is the least suitable soil for the capillary fringe approximation in the VB model. Along B_1B we assumed a no-flow boundary condition and along BC we set up the pressure head p=-40cm. Discretization was as following: the targeted FE size was 0.5 cm, that made the total number of nodes 8420, and 360 1-D and 16718 2-D finite elements.

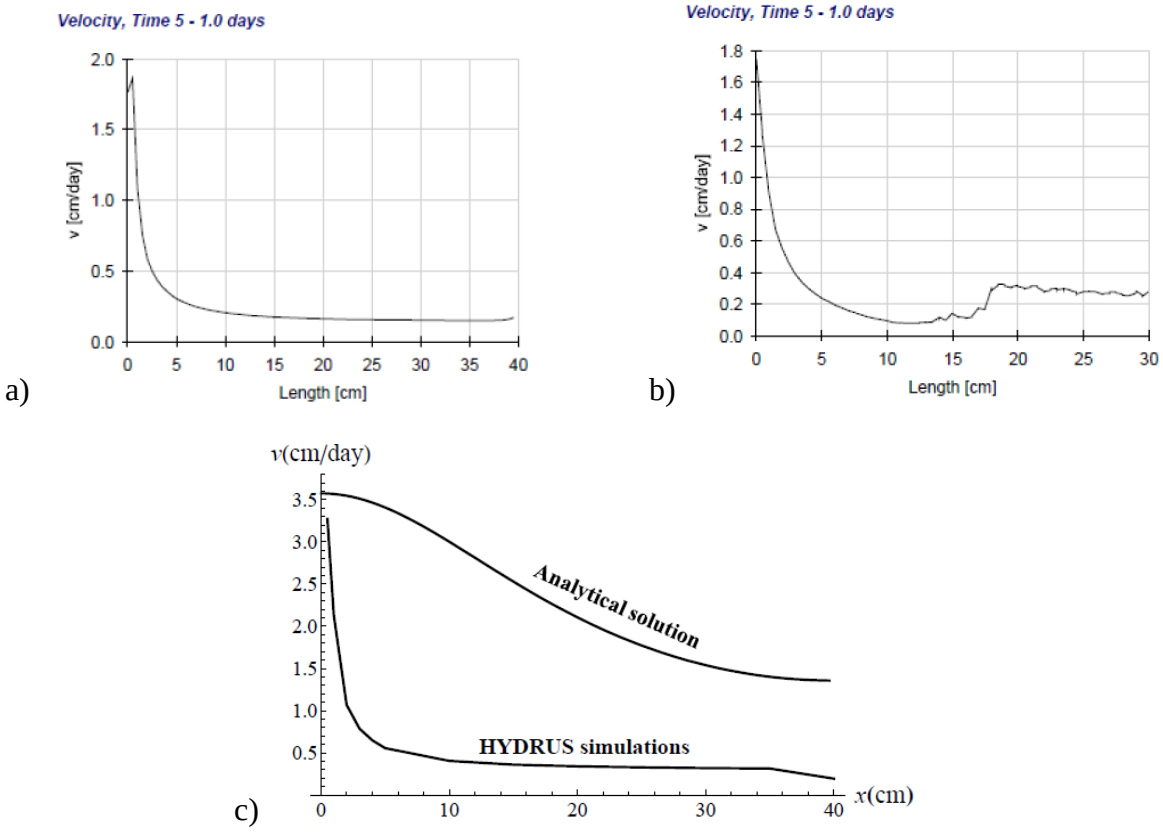

Fig.5. The total HYDRUS velocity along BC at t= 1 day (panel a), HYDRUS velocity across vertical segment AB_1 at t=1 day (panel b), vertical component of velocity at t=0.2 days in HYDRUS and in analytical solution (panel c).

The coloured map in Fig.4a plots isobars at t=1 day, which sandwich the phreatic surface (zero-pressure line) in the two rectangles, with the characteristic points the same as in Fig.1b. Fig.4b shows Fig.4a illustrates that the gravity drainage in a coarse rectangle G_p is indeed almost 1-D while in the left fine-texture triangle the phreatic line is curved. HYDRUS flow is essentially 2-D in G_z, as was the case in the VB model of Section 2. Fig.4b shows contours of the moisture content at t=20 days. They illustrates that the right (mono-coloured) rectangle is indeed tension-saturated but we can not distinguish the phreatic line in this rectangle while in the left rectangle this line is clearly horizontal as in Fig.4a and in the analytical conceptual model of Fig.1b.

Next, we repeated HYDRUS computations for a total duration of 1 day. Fig.5a,b present the distribution of the total HYDRUS velocity along BC and A_1B at t= 1 day. Fig.5cb, shows the vertical component, $v(x)$, of the Darcian velocity computed by HYDRUS for t=0.2 days along BC and the same vertical component analytically computed at the same time by eqns.(14)-(15), which were converted to the same dimensional quantities used in HYDRUS simulations plotted as curve 1 (c=40 cm, d=30 cm, b=5 cm, p_{BC} =40 cm and t=0.05·48/43 days).

Fig.5c shows that the evaporation intensity does spike close to point B (Fig.1b) in both HYDRUS and the analytical solution. The outlet velocity in HYDRUS is lower than predicted by the VB model because the latter assumes the highest (saturated) conductivity for the entire domain (rectangle), whereas HYDRUS tracks explicitly the decreasing hydraulic conductivity with reduced water content. A comparison of Fig.5a and Fig.5c also shows that the Darcian velocity rapidly decreases with time. Fig.5c shows the total HYDRUS velocity along the interface AB_1 between two porous compartments (a bounding streamline in the VB model) at t=1 day. This curve illustrates presence of cross-flow (ignored in the VB model) from G_p to G_z through the segment A_1B. However, at later time (about 4 days, the results are not shown in Fig.5) A_1B in HYDRUS also becomes almost impermeable to cross-flow and water moves horizontally from G_p to G_z mostly via AA_1 that qualitatively agrees with the VB model of Section 2. Eventually, we carried out

simulations for a very early stage of the process (60 minutes). HYDRUS and analytical solution of Section 2 predict that in one hour A_2A_1 drops to the level z_H=23 cm and y=26 cm, respectively. The extinction time in the analytical solution and HYDRUS do not match well: T is less than 1 day and 6 days, respectively. This discrepancy can stem from the already mentioned lower unsaturated hydraulic conductivity of G_z in HYDRUS as compared with the VB model. Additionally, HYDRUS takes into account both capillarity and hydraulic resistance to the drawdown in the coarse (left) rectangle (ignored in the VB model).

4. Time-optimal problem and optimization of texture of soil in wetting against gravity

In Section 2, the initial condition (full saturation) in the fine-textured rectangle, inflow from the coarse-domain and the relatively short duration of evaporation kept a fixed flow domain G_z tension-saturated, while the complex potential domain G_w shrunk that made possible application of the VB model. The transient flow in this model was determined by a time-dependent piezometric head along a dwindling segment of G_z. The 2-D problem in Section 2 was mathematically so complex that our attempts to optimize the aspect ratio of the rectangles in Fig.1b failed. The motivation for solving 1-D optimization problem in this Section is three-fold:

- The GA model, which physically uses the same tension-saturation principle, as the VB model, describes 1-D imbibition against gravity in a homogenous soil from a horizontal water table to an ascending horizontal capillary fringe boundary, i.e. a propagating front; boundary conditions do not depend on time and transiency is determined by time-expansion of the flow domain.

- Best soil texture is analytically found, with an objective to attain the fastest propagation of the front to a specified elevation, or – in a dual formulation – to maximize the height of the front above the water table in a given time.
- HYDRUS1D simulations corroborate analytical optimization.

Application of the solved optimization problem are both in engineering designs and hydrology of natural desert environments. For example, in Muscat (Oman) a major challenge of the last decade is dampening of foundations of buildings caused by a rise of the water table. Evaluation of capillary imbibition into concrete blocks is required. In subsurface irrigation a quasi-horizontal water table is controlled by emitters (Kacimov et al., 2018, Obnosov and Kacimov, 2018) and a target plant roots zone above this zero-pressure line should be wetted in a fastest manner, although the final height of the wetting zone should not approach the soil surface to avoid evaporation. Other technical applications, e.g. in the textile and paper industries, have been addressed by Pan and Zhong (2006), Patnaik et al. (2006), Ruoff et al. (1959), Shou and Fan (2015), Shou et al. (2013).

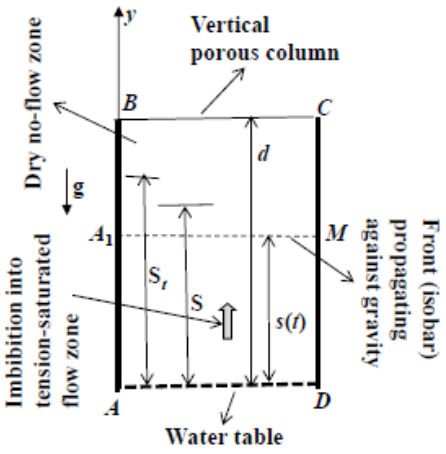

Fig.6. 1-D counter-gravity imbibition with a horizontal GA front rising in a dry vertical column from a horizontal water table.

We consider a porous rectangle *ABCD* made of particles of a diameter d_p (Fig.6), which is a control variable in optimization. At $t<0$ the soil is dry and at $t=0$ the lower side *AD* is brought into contact with a horizontal zero-pressure isobar (water table). Imbibition proceeds at $0 < t < \infty$ with a front A_1M, which - in comport with the GA-VB model - separates a tension-saturated zone beneath from a dry no-flow zone above this moving boundary. Along the frontline positioned at $s(t)$ the pressure head is $p=-p_c(d_p)$=const (for a given texture). Unlike the infiltration described by the GA-VB model (PK-77), in the counter-gravity capillary rise of Fig.6 at $t \to \infty$ the front attains a terminal equilibrium S_t . This soil constant varies from several cm (for gravel) to several meters (for clay) (see Table 5, p.37, PK-77). Obviously, $0< s(t)< S_t$. We assume that the column height in Fig.6 obeys the inequality $d>>S_t$ such that no evaporation or exudation takes place through BC and A_1M. At a time instance $t=T$ the locus of the front is *S*. We neglect soil compaction during wicking (addressed by Ijjas, 1966).

Optimization Problem. Determine the soil textural characteristic d_p which maximizes the height *S* at a given *T*. Or, in a dual formulation, determine the diameter d_p, which minimizes *T* at a given *S*.

This problem generalizes the results of Beyhaghi et al. (2014), who optimized a tension-saturated porous matrix in a steady-state 1-D wicking.

We recall (PK-77) that the total head $h(y,t)$ in a vertically heterogeneous column of Fig.6 is described by the following free boundary problem for a second order nonlinear ODE:

$$k_2(y)\frac{\mathrm{d}^2h(\mathrm{y},t)}{\mathrm{d}y^2}-\frac{\mathrm{d}s(t)}{\mathrm{d}t}\frac{m_2}{k_2(y)}\frac{\mathrm{d}\,[k_2(y)]}{\mathrm{d}y}=0, \qquad (16)$$
$$0 \le h(y,t) \le s(t)-p_c[s(t)]\,, \quad h(0,t)=0,\ \ h(s(t),t)=s(t)-p_c[s(t)]\,,$$

where $k_2(y)$ can be considered as a control function (see e.g. Pontryagin et al., 1962). For a homogeneous column eqn. (16) is integrated once i.e. the dynamics of the front is described by the following Cauchy problem for a first order ODE:

$$m_2 \frac{\mathrm{d}s(t)}{\mathrm{d}t} = k_2 \frac{p_c - s(t)}{s(t)}, \quad \mathrm{s}(0) = 0\ . \tag{17}$$

Integration of eqn.(17) yields:

$$T = \frac{m_2}{k_2}\left(p_c \ln \frac{p_c}{p_c - S} - S \right), \tag{18}$$

where m_2 is effective (fillable) porosity of the soil. In what follows, we assume that m_2 is constant for the variable d_p. This is true if all particles are spherical and the type of regular packing (cubic, hexagonal, or other) is the same. The Soil Catalogue and Rosetta package of HYDRUS also shows that with 5-6 orders of magnitude of variation in k_2 (sand-clay), the value of m_2 remains almost constant.

It is well known (PK-77) that the capillarity and conductivity of porous media scale as

$$p_c = e_1 d_p^{-1}, \quad k_2 = e_2 d_p^2 . \tag{19}$$

In eqn.(19), the scaling constant e_1 depends on the density of water, surface tension and contact angle, which we all assume constant. The factor e_2 (Hazen's or Kozeny-Carman parameter) depends on the water density and viscosity, shape of soil particles and packing. We assume that e_2 is also constant.

We introduce dimensionless quantities: $(T^*,\ S^*,\ D) = (\ Te_2 e_1^{1/2}/m_2\ ,\ S/e_1^{1/2},\ d_p/e_1^{1/2})$. Then eqn.(16) takes the form:

$$T^* = -\frac{1}{D^3}\ln(1 - S^* D) - \frac{S^*}{D^2}, \quad 0 < S^* < 1/D\ . \tag{20}$$

From eqn.(20) the stated optimization problem is routinely solved. Fig.7a illustrates $T^*(D)$ at S^*=0.75,1,1.25 (curves 1-3) with clear global minima. In Fig.7b we plot the graphs $S^*(D)$ at T^*=0.5,1.0, 1.5 (curves 1-3), which manifest the sought global maxima. These extrema are found with the help of the **FindMinimum** and **FindMaximum** routines of *Mathematica.*

Fig.7 illustrates the minima T_m^* of $T^*(D)$ and maxima S_M^* of $S^*(D)$ at discrete values of S^* and T^*, correspondingly. Fig.8 plots the found maxima S_M^* (curve 1) and corresponding particle sizes D_M (curve 2) as continuous functions of T^*. Evidently, the optimal soil of Fig.8 at $T^* \to \infty$ becomes unrealistically fine i.e. $D_M \to 0$ and the front rises to an unrealistic elevation i.e. $S_M^* \to \infty$. From Fig.8, for an arbitrary target time we can find the "best soil" i.e. a particle diameter of the grains, which provides the highest propagation of the GA front against gravity.

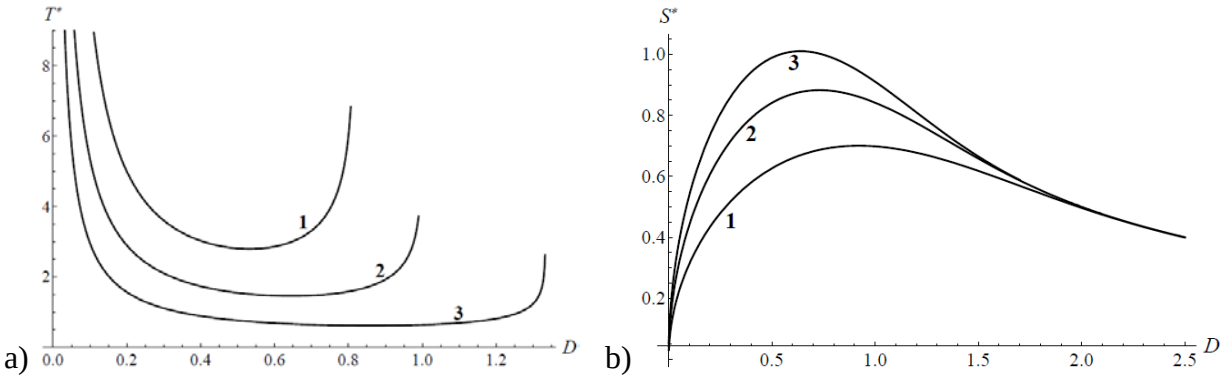

Fig.7. a) Dimensionless time T^* of rise of the GA imbibition front up to a specified target elevation S^*=0.75, 1, and 1.25 (curves 1-3) as function of the particle diameter of the soil; b) Dimensionless front position as a function of the particle size, $S^*(D)$, at three specified time instances T^*=0.5,1.0, and 1.5 (curves 1-3).

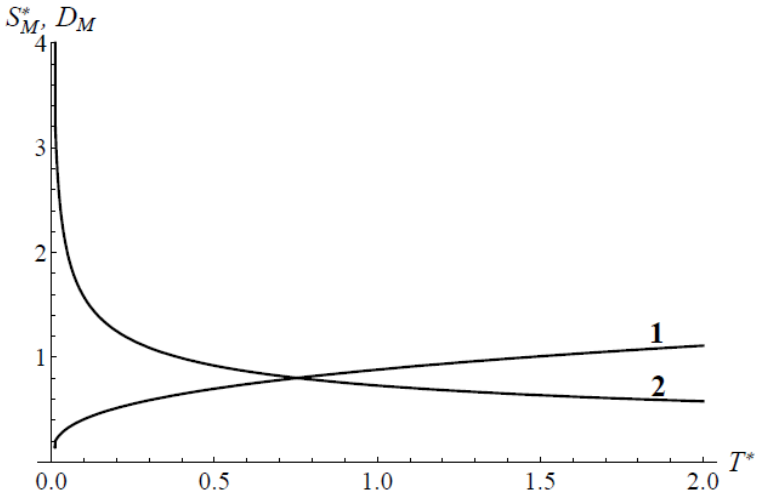

Fig.8. Optima in the dual problem: maximal front loci S_M^* (curve 1) and corresponding particle diameters D_M (curve 2) as functions of T^*.

We also carried out simple HYDRUS simulation for 1-D imbibition depicted in Fig.6. We considered an initially very dry sand, loam and silty clay columns ($m_2=\theta_s$=0.43, 0.43 and 0.36, respectively) from the HYDRUS Soil Catalogue. After 1 day of capillary rise, in the three soils at S=10 cm the volumetric moisture content was about 0.2, 0.4 and 0.17 respectively. This corroborates the analytically proved optimality of a soil (loam), which is not too fine and not too coarse. It is noteworthy that 1-D imbibition into porous columns has been analytically and experimentally studied in terms of the Richards model and two-phase models (see e.g. Alyafei and Blunt, 2018). Evaporative 1-D imbibition with a relatively mild gravity as compared with capillarity is important in studies of damping of foundations of buildings (Navarro et al., 2006).

5. Discussion

The standard perception of evaporation from a horizontal soil surface as a three-stage process with an initial constant rate of evaporation may be misleading as seen in our VB and HYDRUS2D results. Similarly, upscaling-downscaling (Pachepsky and Hill, 2017) of basic hydrological (lump soil water storage in the topsoil of a catchment) or agrophysical (field capacity, wilting point) parameters should be done with care for considering the interactions in the composite domain (Fig.1b) where average properties would not capture the intricacies of soil water dynamics. The patches of conterminous Zones_c – Zones_f sketched in Fig.1b are easily detected in dune landforms shown in Fig.1c for an example in Nambia (see also image 5 in SEF) where accumulation of fine particles in topographic depressions induces formation of ephemeral lakes. Fig.1d shows a satellite

image of dunal lakes, which occurred to be unexpectedly stable after the last Mekuna-Luban cyclones of 2018 (Oman-Saudi Arabia).

An important consideration that is implicit in the VB solution that has not been fully explored in this study is the applicability of the VB model for large scale Sabkha systems (McKay et al. 2016) where all components of the problem remain at play but the interactions occur over kilometer scales (to maintain compatibility with agro-engineering motivation we defer treatment of this companion large scale problem to a future study). We also draw an analogy with other transient flows where the drawdown of water in a highly porous or free-water compartment (reservoir pond, drainage trench, or gravel pack of a well filter) is determined by seepage in an adjacent soil. For example, Philip (1993), Kacimov and Lapin (1993), Kacimov and Yakimov (2009), Kacimov (2000), Maas (2011) Reynolds (2015), Angulo-Jaramillo et al. (2016) presented analytical solutions to similar problems with “naturally” falling-head boundary conditions.

The analytical optimization, which we carried out for 1-D counter-gravity imbibition without evaporation in Section 3 can be applied for 2-D flows in laterally heterogeneous porous composites. Indeed, the four physical factors (gravity, capillary suction, evaporation and Darcian resistance of the matrix, see Beyhaghi et al. 2014) compete and we surmise nontrivial optima from intertwining these factors.

The transient capillary flows studied in this study are relevant to the pioneering but somewhat forgotten Kornev (1935) proposed method for subsurface irrigation from gravel-filled ditches. Kornev (1935), in the context of irrigation engineering promoted the use of soil capillarity as a natural driver for providing uniform wetting to plant root zones (while sheltering water from evaporative losses). In Kornev’s subsurface irrigation design, soil water did not rapidly disappear at the boundaries neither by evaporation nor by deep percolation. By introducing heterogeneous combinations of fine and coarse-textured components of the root zone, Kornev devised means to keep soil moisture “suspended” prolonged its availability and agronomic efficiency.

6. Concluding Remarks

The analytical and numerical solutions for evaporation-induced coupled flows across textural contrasting composite domain (Fig.1b) provide new insights into the combined effects of capillarity and evaporation that persist in the fine-textured domain and drive capillary flow across the domains. Interestingly, the dominance of gravity in the coarse domain (G_p), assists the exchange, whereas in the fine-textured part of the flow domain (G_z) gravity counteracts evaporation-induced upward flow.

The study revisits the VB model of 2-D transient, tension-saturated flows in G_z where no displacement (imbibition) macroscopic front forms. A falling phreatic surface in G_p is similar to one in a "falling-head" permeameter (we ignore Darcian flow losses in this domain). We solved initial-boundary-value problems, by conformal mappings of a constant-size rectangle G_z on a time-shrinking one (G_w in Fig.2a). In the VB model, Laplace's equation for the velocity potential (and stream function) in a flow tube with an equipotential inlet AA_1 enables the analytical machinery of holomorphic functions (PK-77, Strack, 2017). A crucial assumption of the VB model is that the cross flow in Fig.1b from G_p to G_z takes place through a dwindling positive pressure segment AA_1 while a stretching segment BA_1 is a no-flow capillary barrier. We specified a constant pressure head condition along *BC*. If tensiometers or θ-probes supply experimental data on time-decreasing matrix potential or moisture content along *BC*, then a correspondingly increasing function $p_{BC}(t)$, as a boundary condition there, can be introduced in eqn.(13) and in HYDRUS2D.

For the non-linear Richards equation analytical treatment of coupled 2-D flows in G_z - G_p is impossible and we used numerical simulations in HYDRUS2D considering a composite domain (sand-clay), with an isobar *BC* interacting with the atmosphere (Fig.1b) and other boundaries impermeable. The HYDRUS phreatic line consists of a straight horizontal segment A_2A_1

in a sand domain in qualitative agreement with the analytical model, and a curve A_1M in a clay component.

The analytical and numerical 2-D results quantitatively match only at inchoate time i.e. when the composite starts losing water. The vertical component of the Darcian velocity along the outlet boundary *BC* in Fig.1b is higher in the analytical solution, as compared with HYDRUS. The extinction time (when no positive-pressure pore water remains in G_p) is less in the VB analytical model than in HYDRUS. This can be attributed to the difference in the constitutive water relations (step functions for the water retention curve and hydraulic conductivity in the former and the Van Genuchten functions in the latter).

We also extended the steady-state analysis by Beyhaghi et al. (2014) and used 1-D GA-VB model for imbibition from a water table into an initially dry homogenous superjacent soil. Optimization problems were stated and solved by variation of the diameter of the soil particle. Time of front rise at a specified locus and the locus of the front at a specified time were used as criteria in this optimization. The corresponding global minima and maxima are found i.e. a unique soil texture optimizes the front dynamics.

Acknowledgments

This work was funded by a grant from the Sultan Qaboos Higher Center for Culture and Science – Diwan of Royal Court and the Research Council of Oman (TRC) [RC/AGR/SWAE/17/01], SQU grant IG/CAMS/SWAE/18/01 and by the subsidy allocated to Kazan Federal University for the state assignment in the sphere of scientific activities, project № 1.12878.2018/12.1. Helpful comments by three anonymous referees are greatly appreciated.

Data Sharing

The *Mathematica* codes (Sections 2, 4) and HYDRUS project (Section 3) are open files and available to the referees and readers upon request.

7. References

+Abramowitz, M. and Stegun, I.A. 1969. Handbook of Mathematical Functions. Dover, New York.

+Alyafei, N. and Blunt, M.J., 2018. Estimation of relative permeability and capillary pressure from mass imbibition experiments. Advances in Water Resources, 115, 88-94.

+Al-Ismaily, S.S., Al-Maktoumi, A.K., Kacimov, A.R., Al-Saqri, S.M, Al-Busaidi, H.A. and Al-Haddabi, M.H., 2013. A morphed block-crack preferential sedimentation: A smart design and evolution in nature. Hydrological Sciences J., 58 (8), 1779-1788.

+Al-Maktoumi, A., Al-Ismaily, S., Kacimov, A., Al-Busaidi, H., Al-Saqri, S. and Al-Haddabi, M., 2014. Soil substrate as a cascade of capillary barriers for conserving water in a desert environment: lessons learned from arid nature. J. Arid Land, 6(6), 690-703.

+ Angulo-Jaramillo, R., Bagarello, V., Iovino, M. and Lassabatere, L., 2016. Infiltration measurements for soil hydraulic characterization. Springer, Berlin.

+Assouline, S., Narkis, K., Gherabli, R., Lefort, P., and Prat, M., 2014. Analysis of the impact of surface layer properties on evaporation from porous systems using column experiments and modified definition of characteristic length. Water Resources Research, 50(5), 3933-3955.

+Babaev, A.G., 1994. Landscapes of Turkmenistan. In “Biogeography and Ecology of Turkmenistan”, pp. 5-22. Springer, Dordrecht.

+Babaev, A. G. (Ed.), 2012. Desert Problems and Desertification in Central Asia: The Researchers of the Desert Institute. Springer.

+Bagnold, R.A., 1941. The Physics of Blown Sand and Desert Dunes. Methuen, London.

+Benner, E.M. and Petsev, D.N., 2018. Evaporation effect on two-dimensional wicking in porous media. J. of Colloid and Interface Science, 514, 21-29.

+Bechtold, M., Haber-Pohlmeier, S., Vanderborght, J., Pohlmeier, A., Ferré, T.P.A. and Vereecken, H., 2011. Near-surface solute redistribution during evaporation. Geophysical Research Letters, 38(17) L17404.

+Bergstad, M., Or, D., Withers, P.J. and Shokri, N., 2018. Evaporation dynamics and NaCl precipitation on capillarity-coupled heterogeneous porous surfaces. Water Resources Research, 54(6), 3876-3885.

+Beyhaghi, S., Geoffroy, S., Prat, M. and Pillai, K.M., 2014. Wicking and evaporation of liquids in porous wicks: a simple analytical approach to optimization of wick design. AIChE Journal, 60(5), 1930-1940.

+Breckle, S.W., Yair, A. and Veste, M. eds., 2008. Arid Dune Ecosystems: the Nizzana Sands in the Negev Desert (Vol. 200). Springer, Berlin.

+Bouwer, H., 1964. Unsaturated flow in ground-water hydraulics. J. Hydraul. Div. ASCE, 90(5), 121-144.

+Chen, L., Wang, W., Zhang, Z., Wang, Z., Wang, Q., Zhao, M. and Gong, C., 2018. Estimation of bare soil evaporation for different depths of water table in the wind-blown sand area of the Ordos Basin, China. Hydrogeology J., 26, 1693–1704.

+El-Sheikh, M.A., Abbadi, G.A. and Bianco, P.M., 2010. Vegetation ecology of phytogenic hillocks (nabkhas) in coastal habitats of Jal Az-Zor National Park, Kuwait: Role of patches and edaphic factors. Flora. 205(12), 832-840.

+Elizalde, E., Urteaga, R. and Berli, C.L., 2015. Rational design of capillary-driven flows for paper-based microfluidics. Lab on a Chip, 15(10), 2173-2180.

+Erly, L.M., 2012. Reclaiming Native Soil: Cultural Mythologies of Soil in Russia and Its Eastern Borderlands From the 1840s to the 1930s. PhD dissertation, UC Berkeley https://escholarship.org/uc/item/74g4p86x.

+Gael, A. G., and Smirnova, L. F., 1999. Sands and Sandy Soils. Moscow, GEOS (in Russian).

+ Gardner, W. R. and Fireman, M., 1958. Laboratory studies of evaporation from soil columns in the presence of a water table. Soil Science, 85(5), 244-249.

+Geology of the USSR ,1957, Volume 22. Turkmenskaya SSR. Part 1, Geological Description. Ed. N.P.Louppov, Moscow, GNTILGON, (in Russian).

+Hellwig, D. H. R.,1973,. Evaporation of water from sand, 1: Experimental set-up and climatic influences. J. Hydrology, 18(2), 93-108.

+Ijjas, I., 1966. Effect of compactness and initial moisture content of the soil on the process of capillary rise. In “Water in the Unsaturated Zone”, Proceedings of the Wageningen Symposium, Ed. by P.E . Rijtema & H . Wassink, pp. 547-559. UNSECO-IAHS, Printed by Ceuterick, Louvain, Belgium.

+Kacimov, A.R., 2000. Analytic solution for transient flow into a hemispherical auger hole. J. Hydrology, 2000, 228, 1-9.

+Kacimov, A.R., 2006. Capillarity and evaporation exacerbated seepage losses from unlined channels. J. Irrigation and Drainage Engrg. ASCE, 132(6), 623-626.

+Kacimov, A., Al-Issai, J., Al-Amri, M. and Al-Balushi, M., 2010. Green-roof project in Oman: capillary siphoning as a novel and thrifty irrigation technique. Proceedings of the 4rd International Conference on Water Resources and Arid Environments, Riyad, Saudi Arabia, 6-8 Dec, 2010, 479-487.

+Kacimov, A., Al-Maktoumi, A., Al-Ismaily, S., and Al-Busaidi, H., 2017. Moisture and temperature in a proppant-enveloped silt block of a recharge dam reservoir. J. Agricultural and Marine Sciences, 21 (1), 8-17.

+Kacimov, A.R. and Lapin, A.V., 1993. Determination of seepage parameters from data of a quick water intake test and solution of the Boussinesq equation. Power Technology and Engineering, 27(10), 600-607.

+Kacimov, A.R. and Obnosov, Yu.V., 2006. Strip-focused phreatic surface flow driven by evaporation: analytical solution by the Riesenkampf function. Advances in Water Resources, 29, 1565-1571.

+Kacimov, A.R. and Obnosov, Yu.V, 2012. Analytical solutions for seepage near material boundaries in dam cores: the Davison-Kalinin problems revisited. Applied Mathematical Modelling, 36, 1286–1301.

+Kacimov, A.R. and Obnosov, Yu.V., 2013. Pseudo-hysteretic double-front hiatus-stage soil water parcels supplying a plant-root continuum: the Green-Ampt-Youngs model revisited. Hydrological Sciences J., 58(1), 237-248.

+Kacimov, A., Obnosov, Yu.V. and Simunek, J., 2018. Steady flow from an array of subsurface emitters: Kornev's irrigation technology and Kidder's free boundary problems revisited. Transport in Porous Media, 121(3), 643-664.

+Kacimov, A.R., Sherif, M.M., Perret, J.S., and Al-Mushikhi, A., 2009. Control of sea-water intrusion by salt-water pumping: Coast of Oman. Hydrogeology J., 17, 541-558.

+Kacimov, A.R., and Yakimov, N.D., 2001. Moving phreatic surface in a porous slab: an analytical solution. J. Engineering Mathematics, 40, 399-411.

+Kornev, V.G., 1935. Subsurface Irrigation. Selhozgiz, Moscow-Leningrad (in Russian).

+Kunin, V.N., 1959. Local Waters in Deserts and Problems in Their Utilization. Akad. Nauk SSSR, Moscow (in Russian).

+Lehmann, P., Assouline, S., and Or, D., 2008. Characteristic lengths affecting evaporative drying of porous media. Physical Review E - Statistical, Nonlinear, and Soft Matter Physics, 77(5), 056309.

+Lehmann, P., and Or, D., 2009. Evaporation and capillary coupling across vertical textural contrasts in porous media. Physical Review E - Statistical, Nonlinear, and Soft Matter Physics, 80(4),046318.

+Maas, K., 2011. Lek langs de stijgbuis van een put via een slecht afgedichte kleilaag. Water Cycle Research Institute, 31 p. (in Dutch).

+McKay, C.P., Rask, J.C., Detweiler, A.M., Bebout, B.M., Everroad, R.C., Lee, J.Z., Chanton, J.P., Mayer, M.H., Caraballo, A.A., Kapili, B. and Al-Awar, M., 2016. An unusual inverted saline microbial mat community in an interdune sabkha in the Rub'al Khali (the Empty Quarter), United Arab Emirates. PloS One, 11(3), p.e0150342.

+Meng, Q., Cai, Z., Cai, J. and Yang, F., 2019. Oil recovery by spontaneous imbibition from partially water-covered matrix blocks with different boundary conditions. J. of Petroleum Science and Engineering, 172, 454-464.

+Mendez, S., Fenton, E.M., Gallegos, G.R., Petsev, D.N., Sibbett, S.S., Stone, H.A., Zhang, Y. and López, G.P., 2009. Imbibition in porous membranes of complex shape: quasi-stationary flow in thin rectangular segments. Langmuir, 26(2), 1380-1385.

+Navarro, V., Yustres, A., Cea, L., Candel, M., Juncosa, R. and Delgado, J., 2006. Characterization of the water flow through concrete based on parameter estimation from infiltration tests. Cement and Concrete Research, 36(9), 1575-1582.

+Obnosov, Yu.V., and Kacimov, A.R.,2018, Steady Darcian flow in subsurface irrigation of topsoil impeded by substratum: Kornev-Riesenkampf-Philip legacies revisited. Irrigation and Drainage, 67(3), 374-391.

+Ogar, N.P., 2001. Vegetation dynamics on the Syrdarya delta and modern land use. In “Sustainable Land Use in Deserts”, pp. 74-83. Springer, Berlin.

+Orlovsky, L., Matsrafi, O., Orlovsky, N. and Kouznetsov, M., 2012. Sarykamysh lake: collector of drainage water–the past, the present, and the future. In “The Turkmen Lake Altyn Asyr and Water Resources in Turkmenistan”, pp. 107-140. Springer, Berlin.

+Pachepsky, Y. and Hill, R.L., 2017. Scale and scaling in soils. Geoderma, 287, 4-30.

+Pan, N. and Zhong, W., 2006. Fluid transport phenomena in fibrous materials. Textile Progress, 38(2), 1-93.

+Patnaik, A., Rengasamy, R.S., Kothari, V.K. and Ghosh, A., 2006. Wetting and wicking in fibrous materials. Textile Progress, 38(1), 1-105.

+Philip, J.R., 1993. Variable-head ponded infiltration under constant or variable rainfall. Water Resources Research, 29(7), 2155-2165.

+Platonov, A.A. 1934. Takyr. Krasnaya Nov', 9, 82–93 (in Russian).
http://www.rukopisi.imli.ru/rukopis/platonov-andrey-platonovich/takyr-rasskaz-avtograf

+Polubarinova-Kochina, P.Ya., 1977. Theory of Ground Water Movement. Second Edition published in 1977 in Russian, Nauka, Moscow (First Edition published in 1962 in English, Princeton Univ. Press, Princeton).

+Pontryagin, L.S., Boltyanskii, V.G., Gamkrelidze, R.V., and Mishechenko, E.F., 1962. The Mathematical Theory of Optimal Processes. Wiley, New York.

+Prudnikov, A., Brychkov, I. and Marichev, O.,2002. Integrals and Series: Elementary functions. Vol. 1. Fizmtalit, Moscow, Second Edition. (In Russian, Engl. Translation of the First Edition is: New York: Gordon and Breach Science Publishers, 1986).

+Reynolds, W.D., 2015. A generalized variable-head borehole permeameter analysis for saturated, unsaturated, rigid or deformable porous media. Engineering Geology, 185, 10-19.

+Rode, A.A., 1947. The Soil-forming Process and Soil Evolution. Moscow, OGIZ (in Russian). (Engl transl.: Israel Program Sci. Transl., Jerusalem).

+Ruoff, A.L., Prince, D.L., Giddings, J.C. and Stewart, G.H., 1959. The diffusion analogy for solvent flow in paper. Kolloid-Zeitschrift, 166(2), 144-151.

+ Samal, K. P., and Mishra, G. C., 2017. Analysis of seepage from a triangular furrow considering soil capillarity using inverse hodograph and conformal mapping technique. ISH Journal of Hydraulic Engineering, 23(1), 1-12.

+Schulz, S., Horovitz, M., Rausch, R., Michelsen, N., Mallast, U., Köhne, M., Siebert, C., Schüth, C., Al-Saud, M. and Merz, R., 2015. Groundwater evaporation from salt pans: examples from the eastern Arabian Peninsula. J. Hydrology, 531, 792-801.

+Shokri, N., Lehmann, P., and Or, D., 2010. Evaporation from layered porous media. J. Geophysical Research B: Solid Earth, 115(6). B06204.

+Shokri, N., and Or, D., 2011. What determines drying rates at the onset of diffusion controlled stage-2 evaporation from porous media? Water Resources Research, 47(9), W09513.

+Shokri, N. and Or, D., 2013. Drying patterns of porous media containing wettability contrasts. J. Colloid and Interface Science, 391(1), 135-141.

+ Shou, D. and Fan, J., 2015. Structural optimization of porous media for fast and controlled capillary flows. Physical Review E, 91(5), p.053021.

+Shou, D., Ye, L., Fan, J. and Fu, K., 2013. Optimal design of porous structures for the fastest liquid absorption. Langmuir, 30(1), 149-155.

+Šimůnek, J., Van Genuchten, M.T. and Šejna, M., 2016. Recent developments and applications of the HYDRUS computer software packages. Vadose Zone J., 15(7).

+Singer, A., Banin, A., Poberejzsky, L. and Gilenko, M., 2001. Soil crusts in the Amudarya River Delta: properties and formation. In "Sustainable Land Use in Deserts", pp. 103-114. Springer, Berlin.

+Strack, O. D. L., 1978. Distributed sources for unconfined groundwater flow in a half-space. J. Hydrology, 39(3-4), 239-253.

+Strack, O. D. L., 2017. Analytical Groundwater Mechanics. Cambridge Univ. Press.

+Tóth, J. 2009. Gravitational Systems of Groundwater Flow: Theory, Evaluation, Utilization. Cambridge University Press.

+Vedernikov, V.V.,1939. Theory of Seepage and Its Application in Irrigation and Drainage. Gosstrojizdat, Moscow, (in Russian).

+ Youngs, E.G., 2012. Effect of the capillary fringe on steady-state water tables in drained lands. J. of Irrigation and Drainage Eng. ASCE, 138(9), 809-814.

+Youngs, E.G., Elrick, D.E. and Reynolds, W.D., 1993. Comparison of steady flows from infiltration rings in “Green and Ampt” and “Gardner” soils. Water Resources Research, 29(6), 1647-1650.

+Wang, W., Zhang, Z., Yeh, T.C.J., Qiao, G., Wang, W., Duan, L., Huang, S.Y. and Wen, J.C., 2017. Flow dynamics in vadose zones with and without vegetation in an arid region. Advances in Water Resources, 106, 68-79.

+ Willis, W. O., 1960. Evaporation from layered soils in the presence of a water table. Soil Science Society of America J., 24(4), 239-242.

+Wolfram, S., 1991. *Mathematica.* A System for Doing Mathematics by Computer. Addison-Wesley, Redwood City.

+Xiao, J., Stone, H.A. and Attinger, D., 2012. Source-like solution for radial imbibition into a homogeneous semi-infinite porous medium. Langmuir, 28(9), 4208-4212.

+Yechieli, Y. and Wood, W.W., 2002. Hydrogeologic processes in saline systems: playas, sabkhas, and saline lakes. Earth-Science Reviews, 58(3-4), 343-365.

+Zhang, Z., Wang, W., Wang, Z., Chen, L. and Gong, C., 2018. Evaporation from bare ground with different water-table depths based on an in-situ experiment in Ordos Plateau, China. Hydrogeology J., 26, 1683–1691.

+Zonn, I.S. and Esenov, P.E., 2012. The Karakum Desert. In "The Turkmen Lake Altyn Asyr and Water Resources in Turkmenistan", pp. 23-37. Springer, Berlin.

Figure Captions

Fig. 1. Definition sketch, image and photos of spatial zonation in soil texture in arid climates. Plan view, soil surface of a fine-textured Zone$_f$ is wet, coarse-textures soil surface in Zones$_c$ is dry (a); vertical cross-section of two adjacent porous compartments, G_p is a highly porous rectangle in which a horizontal water table drops in 1-D manner and in G_z 2-D tension-saturated transient VB flow takes place (b); interdunal depression in Nambia (c); NASA satellite image visualizing textural intermittence of arid land (d).

Fig.2. Complex potential domain $G_w(t)$ corresponding to G_z (a), image of G_z in the ζ-reference plain (b); image of G_w in the ζ_1-reference plain (c); Soil-water constitutive relations (water retention curve and unsaturated conductivity as function of matrix potential) in VB and VG models (solid and dashed lines) (d).

Fig.3. Dimensionless saturated depth a in G_p as a function of dimensionless time, t, for d =0.75, p_{BC}=1 and three widths of the coarse rectangle b=0.125, 0.25, and 0.5 (curves 1-3 correspondingly).

Fig.4. Pressure head contours at early stage (t=1 day) of drainage of a coarse and imbibition into the fine rectangle a); moisture content contours at late stage (t=20 day) b)

Fig.5. The total HYDRUS velocity along BC at t= 1 day (panel a), HYDRUS velocity across vertical segment AB_1 at t=1 day (panel b), vertical component of velocity at t=0.2 days in HYDRUS and in analytical solution (panel c).

Fig.6. 1-D counter-gravity imbibition with a horizontal GA front rising in a dry vertical column from a horizontal water table.

Fig.7. a) Dimensionless time T^* of rise of the GA imbibition front up to a specified target elevation S^*=0.75, 1, and 1.25 (curves 1-3) as function of the particle diameter of the soil; b) Dimensionless front position as a function of the particle size, $S^*(D)$, at three specified time instances T^*=0.5,1.0, and 1.5 (curves 1-3).

Fig.8. Optima in the dual problem: maximal front loci S_M^* (curve 1) and corresponding particle diameters D_M (curve 2) as functions of T^*.

Abbreviations

GA=Green-Ampt

PK-77=reference to the last (Russian) edition of the Polubarinova-Kochina (1977) book

SEF= Supplementary Electronic File

VB=Vedernikov and Bouwer